ANGULAR RATE ESTIMATION USING AN ARRAY OF FIXED AND VIBRATING TRIAXIAL ACCELERATION MEASUREMENTS

Mark Costello†
Chad Webb‡

Department Of Mechanical Engineering
Oregon State University
Corvallis, Oregon 97331

ABSTRACT

The work reported here describes a method for estimating angular velocity and angular acceleration of a body using clusters of seven triaxial linear acceleration measurements. Four of the triaxial sensors are fixed to the body while three of the sensors vibrate at a constant frequency with respect to the body. Unlike other existing solutions to this problem, the method described here does not require integration and also properly resolves the algebraic sign of the angular rates. After describing the basic method, the paper conducts an error analysis to identify critical design parameters of this sensor concept. The basic algorithm is shown to work well even in the presence of sensor noise, bias and cross axis sensitivity. Practical issues such as the required number of sensors, sensor arrangement, data fusion, and quantization errors are addressed.

SYMBOLS

L_x, L_y, L_z : Components of sensor geometry aligned with a coordinate system fixed to a body.

$\Delta x, \Delta y, \Delta z$: components of position vector in body frame

n_x, n_y, n_z : Vibration amplitudes of vibrating sensors in component directions on a body.

$\omega_x, \omega_y, \omega_z$: Circular Frequency of vibrating sensors in component directions on a body.

ϕ, θ, ψ : Euler roll, pitch and yaw angles of the body

p, q, r : Components of angular velocity in the body reference frame.

$\dot{p}, \dot{q}, \dot{r}$: Components of angular acceleration in the body reference frame.

$\vec{r}_{a \to b}$: Position vector from point a to point b

$\vec{v}_{a/b}, \vec{a}_{a/b}$: Velocity , acceleration vector of point a with respect to reference frame b .

$\vec{\omega}_{a/b}, \vec{\alpha}_{a/b}$: Angular velocity , angular acceleration vector of point a with respect to reference frame b .

F_j, V_j : j^{th} fixed, vibrating sensor

INTRODUCTION

The introduction of a wide variety of microelectromechanical systems (MEMS) into the marketplace has opened the door to incorporate small and relatively inexpensive sensors into air vehicles in new and innovative ways. A case and point is small and medium caliber smart projectiles. Until recently, sensor size, durability, and cost issues have prevented active control of gun launched projectiles. While the development of new MEMS sensors is a very active area of inquiry with new devices entering the marketplace regularly, the most highly developed motion sensor for use on smart weapons is the accelerometer. These devices are particularly attractive for gun launched projectiles since they are rugged and can survive high acceleration levels typical at launch.

† Assistant Professor, Department of Mechanical Engineering, Member AIAA
‡ Graduate Research Assistant, Department of Mechanical Engineering

A number of investigators have examined the use of linear acceleration measurements to compute the angular rates and angular accelerations of a body. See references 1 through 5 for a survery of techniques and applications. Costello and Jitpraphai [6] found that when all acceleration sensors are directly mounted on the body, the algebraic sign of the angular rate components cannot be uniquely determined. The problem of determining the algebraic sign of angular rates can be avoided by using acceleration sensors that are fixed to the body along with acceleration sensors that vibrate in a known manner with respect to the body. Merhav [7] developed a method to estimate body angular rates using 3 single axis, fixed and vibrating acceleration measurements. This technique requires integration over a single vibration period to compute body angular rates. An important side effect of this integration process is the elimination of acceleration measurement bias and noise from the estimation process.

The paper described here presents a new concept for estimating angular velocity and angular acceleration of a body using 4 fixed triaxial acceleration measurements and 3 vibrating triaxial acceleration measurements. The technique has the advantage of not requiring integration while still properly resolving the algebraic sign of the angular rates. The paper begins with a description of the proposed method, followed by a parametric trade study targeted at unveiling the design parameters of this sensor system that affect error propagation.

SYSTEM GEOMETRY

For convenience, the analysis to follow assumes the sensors are arranged in a specific manner. Consider Figure 1 that shows a total of 7 triaxial acceleration sensors mounted to a rigid body. The four sensors depicted as small cubes $\left(F_0, F_1, F_2, F_3\right)$ are fixed to the body. The other three sensors $\left(V_1, V_2, V_3\right)$ depicted as circles oscillate linearly about the center of a line from the origin of the sensor frame $\left(F_0\right)$ to the respective fixed acceleration sensor. Sensors 1, 2, and 3 for both the fixed and vibrating cases lie along the $\vec{I}_S$, $\vec{J}_S$ and $\vec{K}_S$ axes, respectively. The vibrating sensors are positioned a distance L_x, L_y and L_z from the origin of the sensor reference frame and oscillate at a frequency of ω_x, ω_y and ω_z, with an amplitude of n_x, n_y and n_z, respectively.

ANGULAR RATE ESTIMATION USING FIXED AND VIBRATING SINGLE AXIS ACCELERATION SENSORS

The technique developed by Merhav [7] utilizes a set of three fixed and three vibrating single axis acceleration measurements. Referring to Figure 1, sensors F_1, F_2, F_3, V_1, V_2 and V_3 are employed (sensor F_0 at the origin is not required). A key element of this technique is that the single axis acceleration measurement of a vibrating sensor is perpendicular to its direction of motion. It is therefore mounted in such a way that the sensing axis of the accelerometer is perpendicular to the direction of vibrating motion. Acceleration measurements from sensors F_1 and V_1 are along the $\vec{J}_S$ axis while the motion of sensor V_1 is along the $\vec{I}_S$ axis. In the same manner, acceleration measurements from sensors F_2 and V_2 are along the $\vec{K}_S$ axis while the motion of sensor V_2 is along the $\vec{J}_S$ axis. Following this pattern, acceleration measurements from sensors F_3 and V_3 are along the $\vec{I}_S$ axis while the motion of V_3 is along the $\vec{K}_S$ axis.

The acceleration of each vibrating sensor can be computed in terms of the fixed sensor acceleration using the general one point moving on a rigid body formula [8].

$$\begin{aligned} \vec{a}_{V_j/I} &= \vec{a}_{F_j/I} + \vec{a}_{V_j/B} + \vec{\alpha}_{B/I} \times \vec{r}_{F_j \to V_j} \\ &+ \vec{\omega}_{B/I} \times \left(\vec{\omega}_{B/I} \times \vec{r}_{F_j \to V_j} \right) + 2\vec{\omega}_{B/I} \times \vec{v}_{V_j/B} \end{aligned} \tag{1}$$

All terms in Equation (1) are expressed in the sensor reference frame, as shown in Equations (2-8).

$$\vec{a}_{F_j/I} = a_x^{F_j}\vec{I}_s + a_y^{F_j}\vec{J}_s + a_z^{F_j}\vec{K}_s \tag{2}$$

$$\vec{a}_{V_j/I} = a_x^{V_j}\vec{I}_s + a_y^{V_j}\vec{J}_s + a_z^{V_j}\vec{K}_s \tag{3}$$

$$\vec{a}_{V_j/B} = \tilde{a}_x^{V_j}\vec{I}_s + \tilde{a}_y^{V_j}\vec{J}_s + \tilde{a}_z^{V_j}\vec{K}_s \tag{4}$$

$$\vec{\omega}_{B/I} = p\vec{I}_s + q\vec{J}_s + r\vec{K}_s \tag{5}$$

$$\vec{\alpha}_{B/I} = \dot{p}\vec{I}_s + \dot{q}\vec{J}_s + \dot{r}\vec{K}_s \tag{6}$$

$$\vec{r}_{F_j \to V_j} = \Delta x_{F_j \to V_j}\vec{I}_s + \Delta y_{F_j \to V_j}\vec{J}_s + \Delta z_{F_j \to V_j}\vec{K}_s \tag{7}$$

$$\vec{v}_{V_j/B} = \tilde{v}_x^{V_j}\vec{I}_s + \tilde{v}_y^{V_j}\vec{J}_s + \tilde{v}_z^{V_j}\vec{K}_s \tag{8}$$

The tilde (~) symbol used above vector components signifies that the quantity is with respect to the body, and not inertial space. The components of Equation

(1) in the sensor reference frame are provided by Equation (9).

$$\begin{Bmatrix} a_x^{V_j} \\ a_y^{V_j} \\ a_z^{V_j} \end{Bmatrix} = \begin{Bmatrix} a_x^{F_j} \\ a_y^{F_j} \\ a_z^{F_j} \end{Bmatrix} + \begin{Bmatrix} \tilde{a}_x^{V_j} \\ \tilde{a}_y^{V_j} \\ \tilde{a}_z^{V_j} \end{Bmatrix} + 2\begin{bmatrix} 0 & -r & q \\ r & 0 & -p \\ -q & p & 0 \end{bmatrix} \begin{Bmatrix} \tilde{v}_x^{V_j} \\ \tilde{v}_y^{V_j} \\ \tilde{v}_z^{V_j} \end{Bmatrix} + \begin{bmatrix} -q^2-r^2 & pq-\dot{r} & pr+\dot{q} \\ pq+\dot{r} & -p^2-r^2 & qr-\dot{p} \\ pr-\dot{q} & qr+\dot{p} & -p^2-q^2 \end{bmatrix} \begin{Bmatrix} \Delta x_{F_j\to V_j} \\ \Delta y_{F_j\to V_j} \\ \Delta z_{F_j\to V_j} \end{Bmatrix} \tag{9}$$

Harmonic motion of each individual vibrating sensor is along a single axis. Thus the components of the relative position, velocity and acceleration vectors can be expressed as shown in Equations (10-23).

$$\Delta x_{F_2\to V_2} = \Delta x_{F_3\to V_3} = 0 \tag{10}$$
$$\Delta y_{F_1\to V_1} = \Delta y_{F_3\to V_3} = 0 \tag{11}$$
$$\Delta z_{F_1\to V_1} = \Delta z_{F_2\to V_2} = 0 \tag{12}$$
$$\Delta x_{F_1\to V_1} = n_x \sin\left(\omega_x t\right) - L_x \tag{13}$$
$$\Delta y_{F_2\to V_2} = n_y \sin\left(\omega_y t\right) - L_y \tag{14}$$
$$\Delta z_{F_3\to V_3} = n_z \sin\left(\omega_z t\right) - L_z \tag{15}$$
$$\tilde{v}_x^{V_2} = \tilde{v}_x^{V_3} = \tilde{v}_y^{V_1} = \tilde{v}_y^{V_3} = \tilde{v}_z^{V_1} = \tilde{v}_z^{V_2} = 0 \tag{16}$$
$$\tilde{v}_x^{V_1} = n_x\omega_x \cos\left(\omega_x t\right) \tag{17}$$
$$\tilde{v}_y^{V_2} = n_y\omega_y \cos\left(\omega_y t\right) \tag{18}$$
$$\tilde{v}_z^{V_3} = n_z\omega_z \cos\left(\omega_z t\right) \tag{19}$$
$$\tilde{a}_x^{V_2} = \tilde{a}_x^{V_3} = \tilde{a}_y^{V_1} = \tilde{a}_y^{V_3} = \tilde{a}_z^{V_1} = \tilde{a}_z^{V_2} = 0 \tag{20}$$
$$\tilde{a}_x^{V_1} = -n_x\omega_x^2 \sin\left(\omega_x t\right) \tag{21}$$
$$\tilde{a}_y^{V_2} = -n_y\omega_y^2 \sin\left(\omega_y t\right) \tag{22}$$
$$\tilde{a}_z^{V_3} = -n_z\omega_z^2 \sin\left(\omega_z t\right) \tag{23}$$

Extracting the $\vec{I}_S$ axis component of Equation (9) applied to sensors F_3 and V_3, the $\vec{J}_S$ axis component applied to sensors F_1 and V_1, and the $\vec{K}_S$ axis components applied to sensors F_2 and V_2 yields Equation (24).

$$\begin{Bmatrix} a_x^{V_3} \\ a_y^{V_1} \\ a_z^{V_2} \end{Bmatrix} - \begin{Bmatrix} a_x^{F_3} \\ a_y^{F_1} \\ a_z^{F_2} \end{Bmatrix} = \begin{Bmatrix} (pr+\dot{q})(n_z \sin\left(\omega_z t\right) + L_z) \\ (pq+\dot{r})(n_x \sin\left(\omega_x t\right) + L_x) \\ (qr+\dot{p})(n_y \sin\left(\omega_y t\right) + L_y) \end{Bmatrix} + \begin{Bmatrix} 2qn_z\omega_z \cos\left(\omega_z t\right) \\ 2rn_x\omega_x \cos\left(\omega_x t\right) \\ 2pn_y\omega_y \cos\left(\omega_y t\right) \end{Bmatrix} \tag{24}$$

Assume the vibrating sensors operate at a frequency much higher than that of the body, so much so that over a single cycle of sensor vibration, the angular rates are approximately constant and their time derivatives are zero. Multiplying the components of Equation (24) by $\cos\left(\omega_y t\right)$, $\cos\left(\omega_z t\right)$ and $\cos\left(\omega_x t\right)$, respectively, and integrating over a single cycle of sensor vibration isolates the angular velocity components.

$$p = \frac{1}{2\pi n_y} \int_0^{2\pi/\omega_y} \cos\left(\omega_y t\right)(a_z^{V_2} - a_z^{F_2})dt \tag{25}$$
$$q = \frac{1}{2\pi n_z} \int_0^{2\pi/\omega_z} \cos\left(\omega_z t\right)(a_x^{V_3} - a_x^{F_3})dt \tag{26}$$
$$r = \frac{1}{2\pi n_x} \int_0^{2\pi/\omega_x} \cos\left(\omega_x t\right)(a_y^{V_1} - a_y^{F_1})dt \tag{27}$$

Thus, to estimate the angular rate components of a body in the sensor reference frame, three quadratures must be performed using the fixed and vibrating sensor measurements. Note the integrals are closely related to the first cosine wave harmonic amplitude. The difference between the fixed and vibrating accelerations form the multiplicative constant applied to the cosine wave. This technique has the significant advantage that it naturally eliminates sensor bias and noise from the estimates of the angular rate components. To see this, note that sensor bias adds a constant error to the acceleration difference in the integrals above, which, when multiplied by $\cos(\omega_x t)$, $\cos(\omega_y t)$ or $\cos(\omega_z t)$ and integrated over a single cycle of sensor vibration is zero. Sensor noise adds a zero mean random quantity to the acceleration differences in Equations (25-27). This noise, when multiplied by a sinusoid and integrated over a single cycle also yields zero. The disadvantage of this technique is that numerical quadrature must be accurately computed to estimate the angular velocity components. Also, the algorithm was developed based on the assumption that the angular rates are constant over a cycle of the vibrating sensors, thus limiting the useful frequency range of measurement.

ANGULAR RATE ESTIMATION USING FIXED TRIAXIAL ACCELERATION SENSORS

Viewing Figure 1, the technique developed by Costello and Jitpraphia [6] uses four fixed triaxial acceleration sensors. The vibrating acceleration sensors are disregarded. Application of Equation (1) to sensor point combinations $F_0 - F_1$, $F_1 - F_2$ and $F_2 - F_3$ generates three sets of equations which are concatenated into matrix form as shown in Equations (28-31).

$$A = MR \tag{28}$$

$$A = \begin{bmatrix} a_x^{F_0} - a_x^{F_1} & a_x^{F_1} - a_x^{F_2} & a_x^{F_2} - a_x^{F_3} \\ a_y^{F_0} - a_y^{F_1} & a_y^{F_1} - a_y^{F_2} & a_y^{F_2} - a_y^{F_3} \\ a_z^{F_0} - a_z^{F_1} & a_z^{F_1} - a_z^{F_2} & a_z^{F_2} - a_z^{F_3} \end{bmatrix} \tag{29}$$

$$M = \begin{bmatrix} -q^2 - r^2 & -\dot{r} + pq & \dot{q} + pr \\ \dot{r} + pq & -p^2 - r^2 & -\dot{p} + qr \\ -\dot{q} + pr & \dot{p} + qr & -p^2 - q^2 \end{bmatrix} \tag{30}$$

$$R = 2\begin{bmatrix} -L_x & L_x & 0 \\ 0 & -L_y & L_y \\ 0 & 0 & -L_z \end{bmatrix} \tag{31}$$

The matrix A is populated by sensor measurements and is known at each discrete time instant. The distance matrix R is defined by sensor geometry and the matrix M contains the unknown quantities that are to be estimated. Provided the distance matrix R is nonsingular, the matrix M can be computed. Previous efforts have yielded algorithms to compute angular rate components using the elements of the M matrix [2,3,6].

$$p = s_p\left[\tfrac{1}{2}\left(\left(M_{1,1} - M_{2,2}\right)^2 + \left(M_{1,2} + M_{2,1}\right)^2\right)^{\frac{1}{2}} + \tfrac{1}{2}\left(M_{1,1} - M_{2,2}\right)\right]^{\frac{1}{2}} \tag{32}$$

$$q = s_q\left[\tfrac{1}{2}\left(\left(M_{1,1} - M_{2,2}\right)^2 + \left(M_{1,2} + M_{2,1}\right)^2\right)^{\frac{1}{2}} - \tfrac{1}{2}\left(M_{1,1} - M_{2,2}\right)\right]^{\frac{1}{2}} \tag{33}$$

$$r = s_r\left[\tfrac{1}{2}\left(\left(M_{1,1} - M_{2,2}\right)^2 + \left(M_{1,2} + M_{2,1}\right)^2\right)^{\frac{1}{2}} - \tfrac{1}{2}\left(M_{1,1} + M_{2,2}\right)\right]^{\frac{1}{2}} \tag{34}$$

where s_p, s_q, s_r are the sign of p, q, r. Angular rate estimation using only fixed triaxial acceleration measurement is sensitive to acceleration measurement noise, particularly for some critical combinations of sensor geometry and angular rates. Moreover, the algebraic sign of the angular rates cannot be ascertained using only fixed triaxial acceleration measurement as two valid solutions exist.

ANGULAR RATE ESTIMATION USING FIXED AND VIBRATING TRIAXIAL ACCELERATION SENSORS

Again consulting Figure 1, consider estimating angular rates using fixed and vibrating triaxial acceleration sensors. Applying Equation (1) to each fixed and rotating point combination yields Equation (35).

$$\tilde{A} = M\tilde{R} + 2S\tilde{V} \tag{35}$$

$$\tilde{A} = \begin{bmatrix} a_x^{V_1} - a_x^{F_1} - \tilde{a}_x^{V_1} & a_x^{V_2} - a_x^{F_2} - \tilde{a}_x^{V_2} & a_x^{V_3} - a_x^{F_3} - \tilde{a}_x^{V_3} \\ a_y^{V_1} - a_y^{F_1} - \tilde{a}_y^{V_1} & a_y^{V_2} - a_y^{F_2} - \tilde{a}_y^{V_2} & a_y^{V_3} - a_y^{F_3} - \tilde{a}_y^{V_3} \\ a_z^{V_1} - a_z^{F_1} - \tilde{a}_z^{V_1} & a_z^{V_2} - a_z^{F_2} - \tilde{a}_z^{V_2} & a_z^{V_3} - a_z^{F_3} - \tilde{a}_z^{V_3} \end{bmatrix} \tag{36}$$

where the matrix M is given by Equation (30).

$$\tilde{R} = \begin{bmatrix} n_x \sin(\omega_x t) - L_x & 0 & 0 \\ 0 & n_y \sin(\omega_y t) - L_y & 0 \\ 0 & 0 & n_z \sin(\omega_z t) - L_z \end{bmatrix} \tag{37}$$

$$\tilde{V} = \begin{bmatrix} n_x\omega_x \cos(\omega_x t) & 0 & 0 \\ 0 & n_y\omega_y \cos(\omega_y t) & 0 \\ 0 & 0 & n_z\omega_z \cos(\omega_z t) \end{bmatrix} \tag{38}$$

$$S = \begin{bmatrix} 0 & -r & q \\ r & 0 & -p \\ -q & p & 0 \end{bmatrix} \tag{39}$$

Solving for S yields Equation (40),

$$S = \frac{1}{2}\left(\tilde{A} - AR^{-1}\tilde{R}\right)\tilde{V}^{-1} \tag{40}$$

which is utilized to compute the components of the angular rate vector. Solving for the angular rates yields:

$$\begin{aligned} p = {} & \frac{\left(a_z^{F_2} - a_z^{F_0}\right)\left(L_y - n_y \sin\left(\omega_y t\right)\right) + 2L_y\left(a_z^{V_2} - a_z^{F_2}\right)}{8L_y n_y \omega_y \cos\left(\omega_y t\right)} \\ & - \frac{\left(a_y^{F_3} - a_y^{F_0}\right)\left(L_z - n_z \sin\left(\omega_z t\right)\right) + 2L_z\left(a_y^{V_3} - a_y^{F_3}\right)}{8L_z n_z \omega_z \cos\left(\omega_z t\right)} \end{aligned} \tag{41}$$

$$\begin{aligned} q = {} & \frac{\left(a_x^{F_3} - a_x^{F_0}\right)\left(L_z - n_z \sin\left(\omega_z t\right)\right) + 2L_z\left(a_x^{V_3} - a_x^{F_3}\right)}{8L_z n_z \omega_z \cos\left(\omega_z t\right)} \\ & - \frac{\left(a_z^{F_1} - a_z^{F_0}\right)\left(L_x - n_x \sin\left(\omega_x t\right)\right) + 2L_x\left(a_z^{V_1} - a_z^{F_1}\right)}{8L_x n_x \omega_x \cos\left(\omega_x t\right)} \end{aligned} \tag{42}$$

$$\begin{aligned} r = {} & \frac{\left(a_y^{F_1} - a_y^{F_0}\right)\left(L_x - n_x \sin\left(\omega_x t\right)\right) + 2L_x\left(a_y^{V_1} - a_y^{F_1}\right)}{8L_x n_x \omega_x \cos\left(\omega_x t\right)} \\ & - \frac{\left(a_x^{F_2} - a_x^{F_0}\right)\left(L_y - n_y \sin\left(\omega_y t\right)\right) + 2L_y\left(a_x^{V_2} - a_x^{F_2}\right)}{8L_y n_y \omega_y \cos\left(\omega_y t\right)} \end{aligned} \tag{43}$$

Using the angular rates from Equations (41-43) and the matrix M of Equation (28) which employs only the fixed triaxial sensors F_1, F_2, F_3, the angular acceleration components can be determined as well.

$$\dot{p} = \frac{1}{4L_y L_z}\left[L_z\left(a_z^{F_2} - a_z^{F_0}\right) - L_y\left(a_y^{F_3} - a_y^{F_0}\right)\right] \tag{44}$$

$$\dot{q} = \frac{1}{4L_x L_z}\left[L_x\left(a_x^{F_3} - a_x^{F_0}\right) - L_z\left(a_z^{F_1} - a_z^{F_0}\right)\right] \tag{45}$$

$$\dot{r} = \frac{1}{4L_x L_y}\left[L_y\left(a_y^{F_1} - a_y^{F_0}\right) - L_x\left(a_x^{F_2} - a_x^{F_0}\right)\right] \tag{46}$$

It should be noted that in comparison to the method developed by Merhav [7], the method described here requires more sensors, but does not require integration over a cycle of vibration. Furthermore, it makes no assumptions about the angular rates as constant over a single cycle of sensor vibration, extending the range of usable frequency band of the method. However, in computing the angular rates p, q and r, a problem arises as the combination of ωt approaches an odd multiple of $\frac{\pi}{2}$, where $\cos\left(\omega t\right) = 0$ and the solutions listed in Equations (41-43) become singular. This problem is overcome by sampling the data in such a way that the combination of ωt is always nearly a common multiple of π so that $\cos\left(\omega t\right) \approx \pm 1$. This requires knowledge of the oscillation frequency and the sampling rate of data collection.

ACCELEROMETER MODEL

In order to investigate the performance of the proposed algorithm in the presence of inaccurate and realistic acceleration measurements, simulated acceleration readings that include noise, bias, cross-axis sensitivity, and scale factor errors are analyzed. Furthermore, accelerometers sense gravity, so this effect is present in the readings and must be subtracted to obtain the acceleration readings. A triaxial acceleration measurement is modeled as

$$\begin{aligned} \begin{Bmatrix} \tilde{a}_{x_i} \\ \tilde{a}_{y_i} \\ \tilde{a}_{z_i} \end{Bmatrix}_{Sensed} = {} & \begin{bmatrix} S_{xx_i} & C_{xy_i} & C_{xz_i} \\ C_{xy_i} & S_{yy_i} & C_{yz_i} \\ C_{xz_i} & C_{yz_i} & S_{zz_i} \end{bmatrix} \left(\begin{Bmatrix} \tilde{a}_{x_i} \\ \tilde{a}_{y_i} \\ \tilde{a}_{z_i} \end{Bmatrix} - g \begin{Bmatrix} -s_\theta \\ s_\phi c_\theta \\ c_\phi c_\theta \end{Bmatrix} \right) \\ & + \begin{Bmatrix} \tilde{a}_{x_i} \\ \tilde{a}_{y_i} \\ \tilde{a}_{z_i} \end{Bmatrix}_{Noise} + \begin{Bmatrix} \tilde{a}_{x_i} \\ \tilde{a}_{y_i} \\ \tilde{a}_{z_i} \end{Bmatrix}_{Bias} \end{aligned} \tag{47}$$

in which $S_{xx_i}, S_{yy_i}, S_{zz_i}$ are orthogonal components of the scale factor for the i^th accelerometer and $C_{xy_i}, C_{xz_i}, C_{yz_i}$ represent components of cross axis sensitivity for the same accelerometer.

Data acquisition also poses a threat to acceleration measurement integrity. Voltage measurements are digitized, leading to quantization error caused by the A/D converter. The smallest incremental voltage signal that can be represented after A/D conversion is referred to as the quantization level. It is proportional to the voltage range and the number of bits of the A/D converter. Under the assumption that the 2's complement scheme of binary coding is used , the quantization level is [9]:

$$q = \frac{V_{fs}}{2^n} \tag{48}$$

where n is the number of bits and V_{fs} is the full scale voltage. Equation (48) illustrates the smallest voltage increment a given A/D converter can represent. Thus, a 0-8V, 4 bit A/D converter would have a quantization level of 0.5V. The quantized acceleration reading takes into account the quantization level and the scale factor of the accelerometer.

$$a_q = \frac{q}{S_j} \tag{49}$$

The difference between true and quantized acceleration readings represents the acceleration error caused by A/D conversion.

ERROR ANALYSIS

If $L_x = L_y = L_z = L$ and $n_x = n_y = n_z = n$ and, in addition, the data is sampled as described previously, then Equations (41-43) reduce to

$$p = \frac{a_y^{F_0} + a_y^{F_3} - 2a_y^{V_3}}{8n\omega} - \frac{a_z^{F_0} + a_z^{F_2} - 2a_z^{V_2}}{8n} \tag{50}$$

$$q = \frac{a_z^{F_0} + a_z^{F_1} - 2a_z^{V_1}}{8n\omega} - \frac{a_x^{F_0} + a_x^{F_3} - 2a_x^{V_3}}{8n} \tag{51}$$

$$r = \frac{a_x^{F_0} + a_x^{F_2} - 2a_x^{V_2}}{8n\omega} - \frac{a_y^{F_0} + a_y^{F_1} - 2a_y^{V_1}}{8n} \tag{52}$$

Notice the linear dependence of the solution on the acceleration measurements. Thus, the structure of error propagation from accelerometer error to angular rate estimation error can be represented using a linear function. The dependence of the solution on error in sensor vibration amplitude takes on the form of $\frac{C}{(n+n_{error})}$ where C is a constant, while the dependence of the solution on error in vibration frequency is $C_0 + \frac{C_1}{(\omega+\omega_{error})}$ where C_0 and C_1 are also constants. The solution for p, q, r does not depend on the length L.

SENSOR FUSION

The algorithm discussed can be employed to estimate angular rates and accelerations using multiple clusters of sensors. The benefit of using multiple clusters is the inherent smoothing of the output data in the presence of errors. In the simplest case, the sensor cube in Figure 1 could have m cubes packed on either side of it. A more efficient use of space is that illustrated by Figure 2, where each cube in the figure is not only packed end to end, but also contains two sensor clusters at each location; one in the original orientation and the other rotated as shown. For each cluster, an estimate of the angular velocity and angular acceleration is computed. Performing this operation for all m clusters and averaging the results produces an overall estimate of the angular velocity and angular acceleration of the body.

EXAMPLE RESULTS

In order to exercise the algorithm developed above, the algorithm is used to estimate angular rates of a rocket in atmospheric flight. The rocket trajectories to follow are generated from a 6 degree of freedom projectile simulation utilizing a 2-inch square sensor cube and vibrating sensors having an oscillation frequency of 1000 Hz and amplitude of vibration of 0.1 inches. See reference 10 for details of the projectile simulation Normally distributed random noise, with a standard deviation of 50 mg's (1.61 ft/s^2), is added to each acceleration measurement. Furthermore, cross axis sensitivity is set to zero mean with a standard deviation of 1%. The scale factor error has a 3% standard deviation from unity. A 12 bit A/D converter is used, with an accelerometer scale factor of 200mV/g. 500 clusters are employed.

Figures 3-5 provide estimation results for the trajectory of a generic direct fire rocket in the first 0.25 seconds of atmospheric flight. As shown in Figures 3 and 4, roll and pitch rates are very accurately estimated. Figure 5 indicates that yaw rate is slightly biased. This is caused by scale factor error and cross axis sensitivity, both of which equally contribute to estimation errors.

Roll acceleration is poorly predicted (Figure 6). This large error stems from $a_z^{F_0}$ and $a_z^{F_2}$ in Equation (44), which are equal and opposite, so in the absence of error, they cancel out. For a projectile spinning at a high rate, the magnitude of these accelerations are large, compared to the magnitudes of $a_y^{F_0}$ and $a_y^{F_3}$. A small percentage of unbalance between these accelerations is sufficient to cause large estimation errors.

Pitch and yaw accelerations shown in Figures 7-8 are also very sensitive to error. They have significant bias, but take on the same oscillatory motion as the actual data.

In order to understand the benefit of employing many clusters, Figures 9-14 plot the mean absolute value of the error for $p, q, r, \dot{p}, \dot{q}$ and $\dot{r}$ as a function of time after launch for sensor configurations with $2, 10, 100, 500$ clusters. The mean absolute value of error is computed by averaging 20 exemplar rocket trajectories with an impact point CEP of 2.62m at a range of 250m. As would be expected, estimation eror is reduced as the number of sensor clusters is increased. Also, estimation error is reduced as the projectile flies downrange due to reduced projectile spin rate leading to a reduced effect from cross axis sensitivity.

Comparing the roll error plot of Figure 9 to the trajectory simulation of Figure 3, it is clear that the roll error is a very small portion of the total roll rate, nearly regardless of the number of clusters used. This is not the case for pitch and yaw rates. Figures 10 and 11 indicate that a larger number of clusters is necessary to provide error levels that are much smaller than the total signal. On the other hand, angular accleration estimates are poor, even with 500 clusters.

In order to consider the effect of different accelerometer error components on angular rate and acceleration estimation, a breakdown of the errors is shown in Figures 15-20 for the 2 cluster sensor configuration. To generate these results, all accelerometer errors were nulled, except for the error source under consideration. The same exemplar trajectories used for Figures 8-14 were used in Figures 15-20. Examining the roll rate error, it is clear that accelerometer scale factor dominates the total error. Pitch and yaw rate error properties (Figures 16 and 17) are also significantly effected by scale factor errors, but also by accelerometer cross axis sensitivity as well. The angular acceleration estimates (Figures 18,19 and 20) are also dominated by accelerometer scale factor and cross axis sensitivity as well.

A similar trend is evident with larger numbers of sensor clusters as well, but with overall error magnitudes reduced.

CONCLUSION

A method for estimating angular rates and angular acceleration of a body using clusters of seven triaxial linear acceleration measurements is developed and exercised. The method employs four triaxial accelerometers fixed to the body and three triaxial accelerometers that vibrate at a constant frequency with respect to the body. While other solutions to this problem exist, the method reported here is unique in that it does not require integration and also properly resolves the algebraic sign of the angular rates. When applying this estimation technique to an atmospheric rocket, it is shown that the method adequately estimates rocket angular rates in the presence of realistic accelerometer errors, including noise, bias, scale factor, and cross axis sensitivity. Angular acceleration components are poorly estimated. It is also shown that using this algorithm with many clusters of sensors effectively reduces estimation error. Cross axis sensitivity and scale factor error are the driving accelerometer errors that induce large estimation errors for both angular rates and angular acceleration.

REFERENCES

1. J. Genin, J. Hong, W. Xu, "Accelerometer Placement For Angular Velocity Determination," *Journal of Dynamics Systems, Measurement and Control*, Vol. 119, No. 3, 1997, pp. 474-477.
2. J. Angeles, "Computation of Rigid Body Angular Acceleration from Point-Acceleration Measurements," *ASME Journal of Dynamics Systems, Measurement, and Control*, Vol. 109, 1987, pp. 124-127.
3. G.S. Nusholtz, "Geometric Methods in Determining Rigid Body Dynamics," *Experimental Mechanics*, Vol. 33, No. 2, pp. 153-158, 1993.
4. A. J. Padgaonkar, K.W. Krieger, and A.I. King, "Measurement of Angular Acceleration of a Rigid Body Using Linear Accelerometers," *Journal of Applied Mechanics*, Vol. 42, No.3, 1975, pp. 552-556.
5. T.E. Harkins, T.G. Brown, "Practicability Issues In Deriving Angular Rates From Accelerometer Data For The 2.75-Inch MK66 Rocket, "U.S Army Research Lab., Rept. ARL-MR-392, Aberdeen Proving Ground, MD, 1998.
6. M. Costello, T. Jitpraphai, "Determining Angular Velocity and Angular Acceleration of Projectiles Using Triaxial Acceleration Measurements," *Journal of Spacecraft and Rockets*, Vol. 39, No 1, 2002, pp. 73-80.
7. S. Merhav, "A Nongyroscopic Inertial Measurement Unit," *Journal of Guidance, Control and Dynamics*, Vol. 5, No 3, 1982, pp. 227-235.
8. J. Ginsberg, Advanced Engineering Dynamics, ISBN 0-521-47021-8, Cambridge University Press, U.S.A., 1995, pp. 85-88.

9. R. Jacquot, Modern Digital Control Systems, ISBN 0-8247-8914-8, Marcel Dekker, Inc., U.S.A., 1995, pp. 206-209.

10. B. Burchett, M. Costello, "Model Predictive Lateral Pulse Jet Control of an Atmospheric Rocket," *Journal of Guidance, Control and Dynamics,* Vol. 25, No 5, 2002, pp. 860-867.

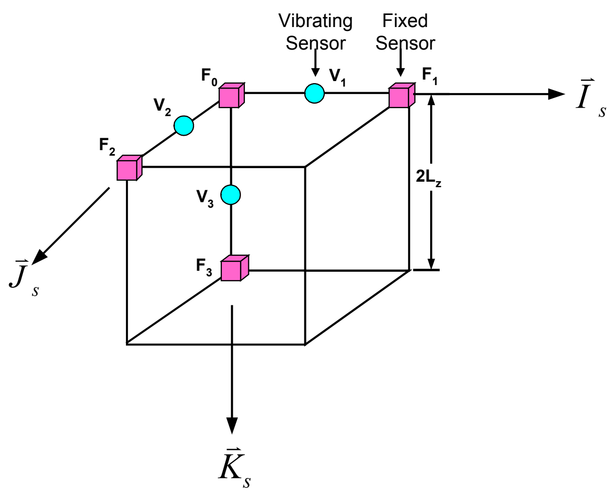

Figure 1 – Sensor Cube Geometry

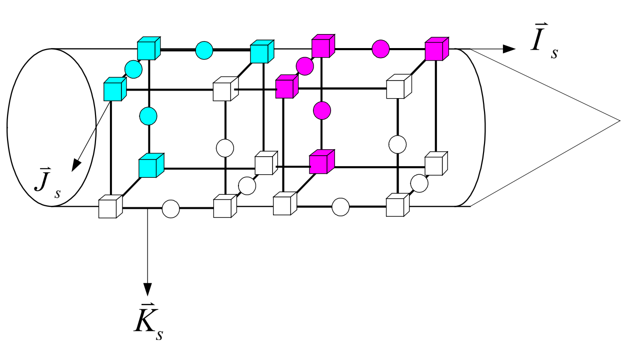

Figure 2. Cluster Layout

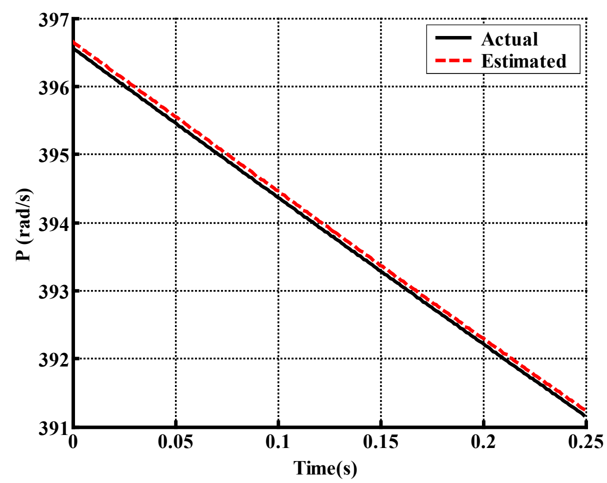

Figure 3. Estimated Roll Rate versus Time.

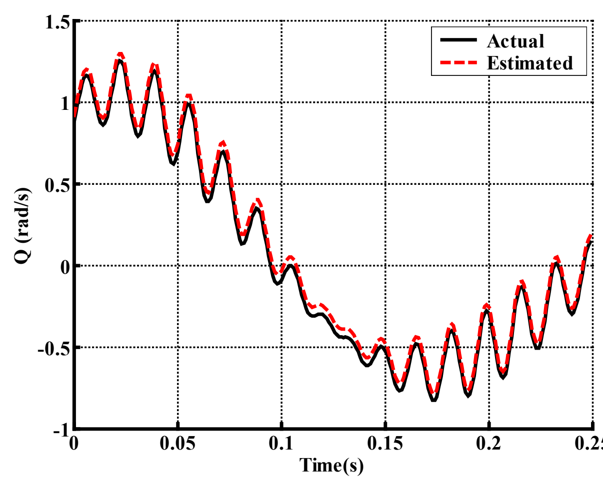

Figure 4. Estimated Pitch Rate versus Time.

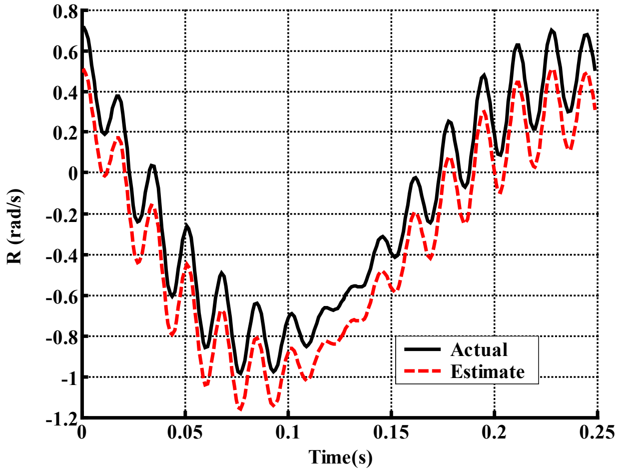

Figure 5. Estimated Yaw Rate versus Time.

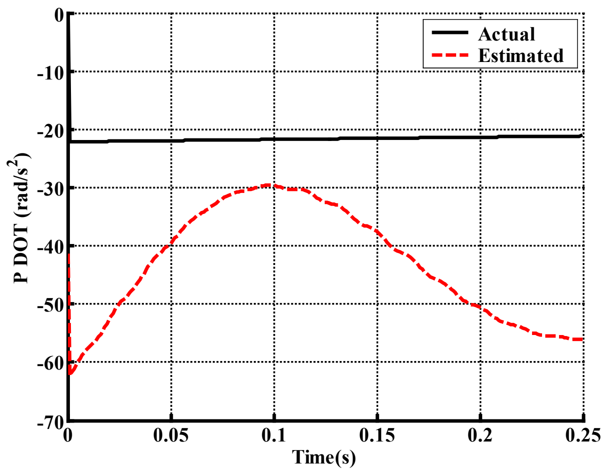

Figure 6. Estimated Roll Acceleration versus Time.

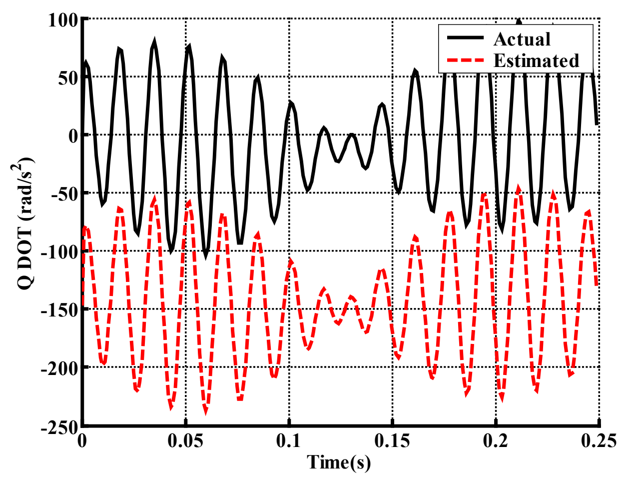

Figure 7. Estimated Pitch Acceleration versus Time.

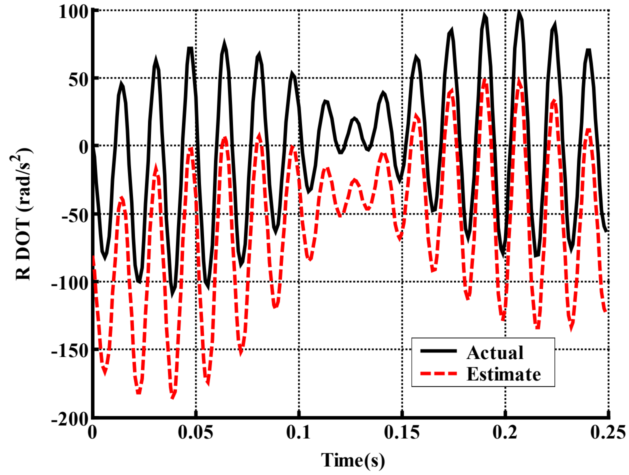

Figure 8. Estimated Yaw Acceleration versus Time.

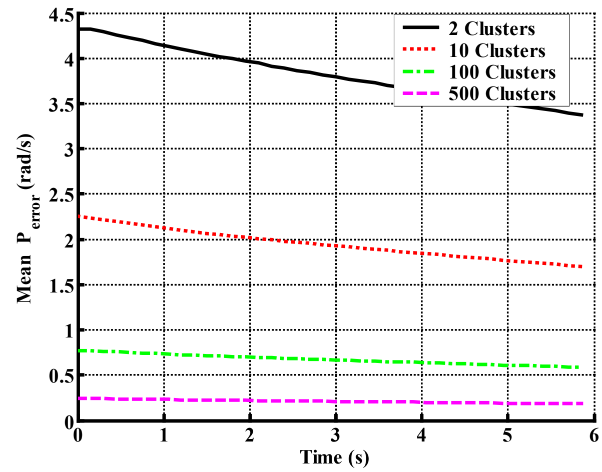

Figure 9. Mean Roll Rate Error versus Time.

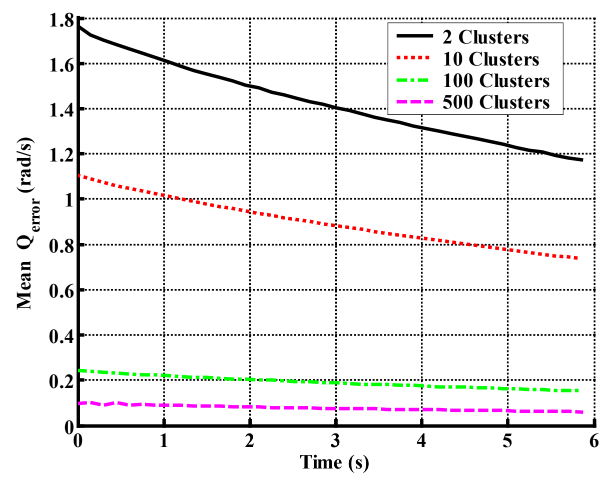

Figure 10. Mean Pitch Rate Error versus Time.

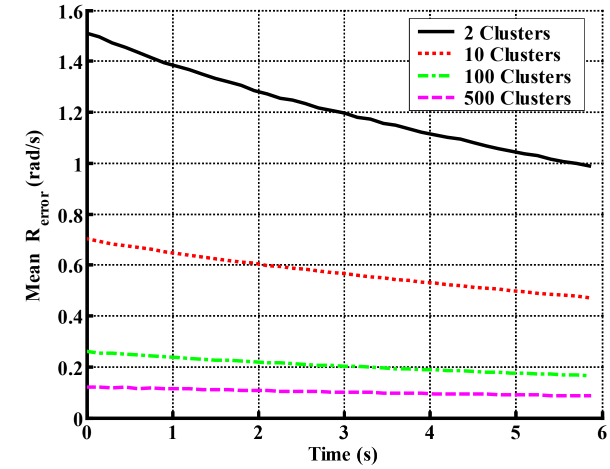

Figure 11. Mean Yaw Rate Error versus Time.

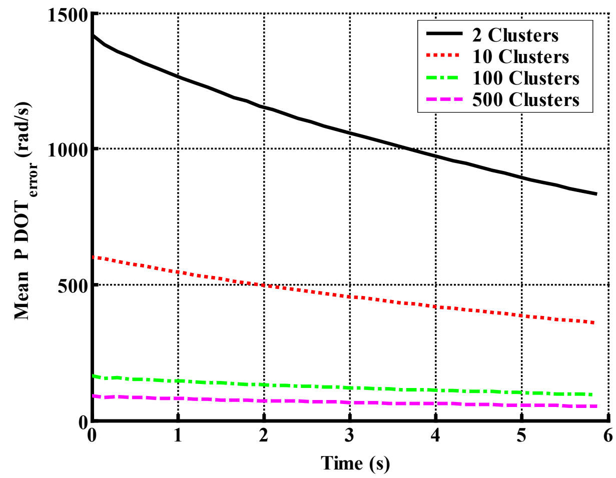

Figure 12. Mean Roll Acceleration Error versus Time.

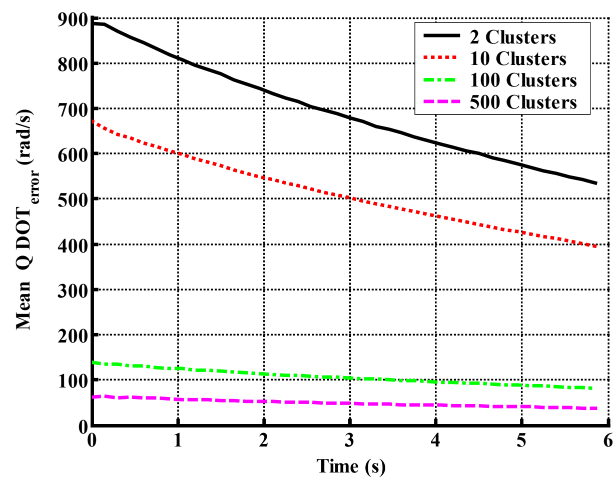

Figure 13. Mean Pitch Acceleration Error versus Time.

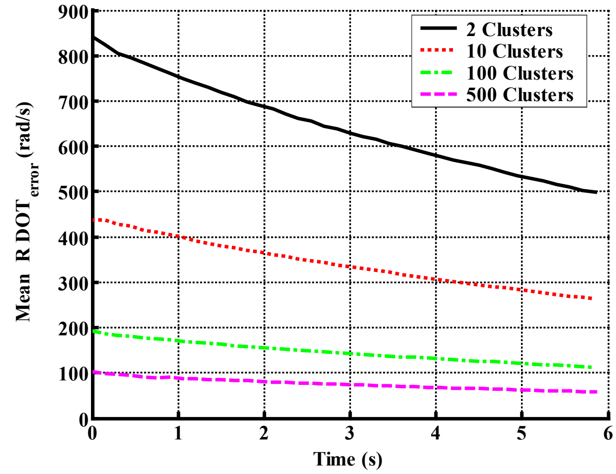

Figure 14. Mean Yaw Acceleration Error versus Time.

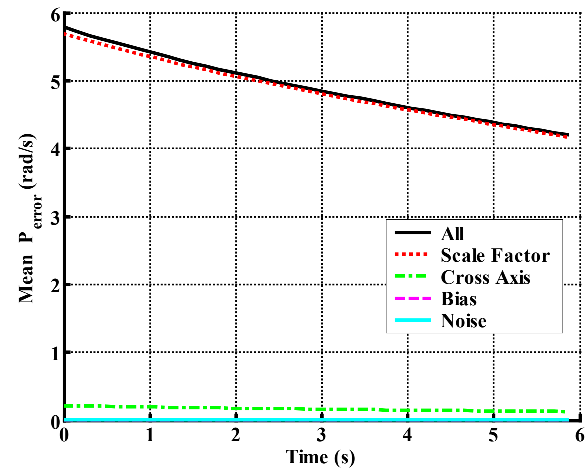

Figure 15. Components Of Roll Rate Error For 2 Cluster Arrangement versus Time.

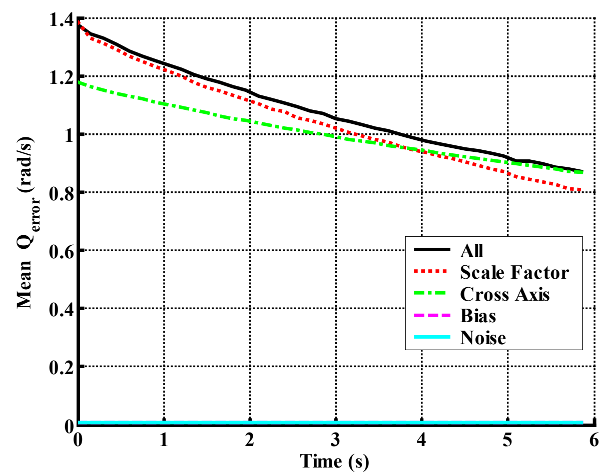

Figure 16. Components Of Pitch Rate Error For 2 Cluster Arrangement versus Time.

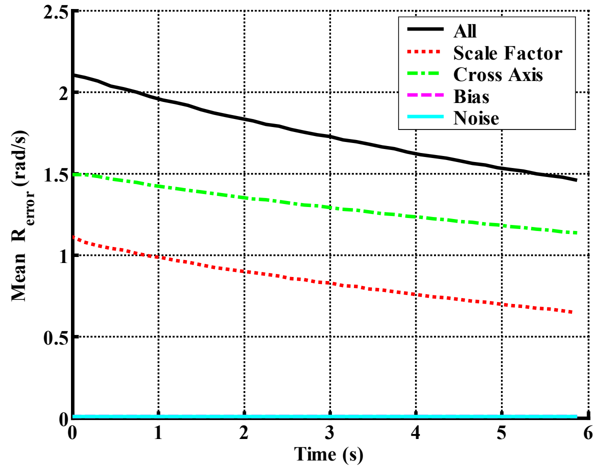

Figure 17. Components Of Yaw Rate Error For 2 Cluster Arrangement versus Time.

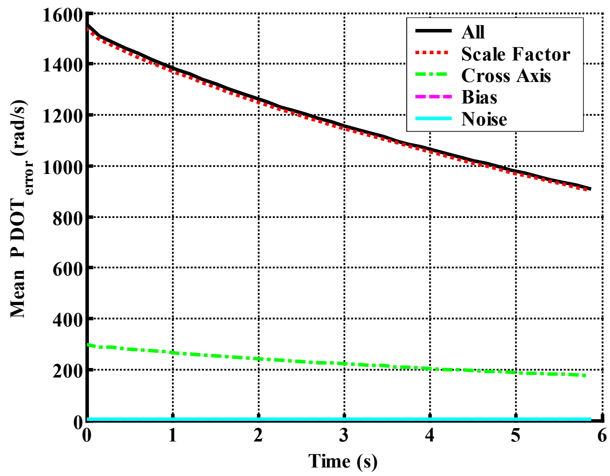

Figure 18. Components Of Roll Acceleration Error For 2 Cluster Arrangement versus Time.

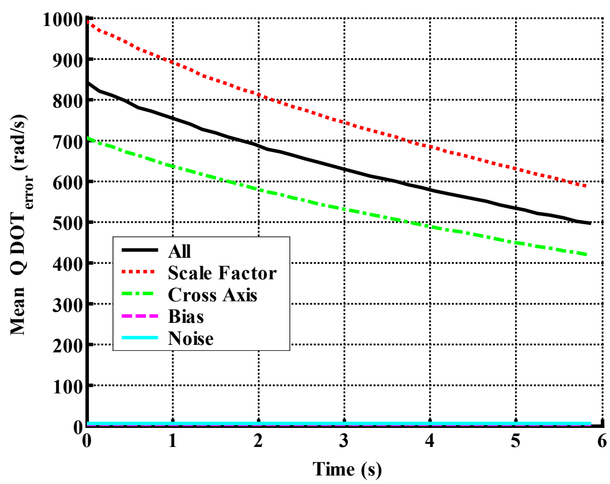

Figure 19. Components Of Pitch Acceleration Error For 2 Cluster Arrangement versus Time.

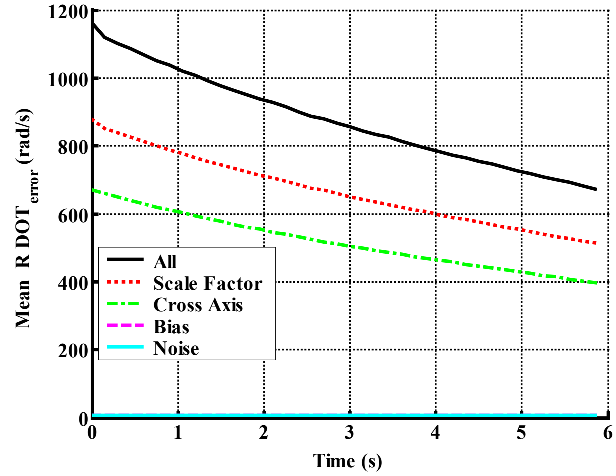

Figure 20. Components Of Yaw Acceleration Error For 2 Cluster Arrangement versus Time.